Conversion of laser light into x rays in thin foil targets

P. Celliers* and K. Eidmann
Max-Planck-Institut für Quantenoptik, D-8046 Garching, Federal Republic of Germany
(Received 22 August 1989)

Planar gold layers of thickness 50–200 nm, both free-standing and supported on substrates of 1-μm polypropylene, were irradiated with 3-ns laser pulses of 0.53 μm wavelength at 10^{12} and 10^{13} W/cm^2. The x-ray emission from the rear and front of the target was measured with symmetrically placed x-ray diodes and x-ray transmission grating film spectrometers. The transmitted laser light was also monitored. Under optimized conditions it is possible to obtain up to 30% conversion of the laser energy in the form of soft x rays from the rear surface of the target with less than 2% laser light transmission. The measured overall conversion efficiency is approximately in agreement with hydrodynamic simulations. The spectral and temporal features of the emission are discussed with respect to the opacity of the hot dense target material.

I. INTRODUCTION

The intense emission of soft x rays from laser-irradiated plasmas is of interest for a variety of applications, such as in indirect drive laser fusion,[1] as a heating and diagnostic tool for investigations of hot compressed matter,[2–5] as a pump source for x-ray lasers,[6] and as an emission source for microlithography.[7,8] Thorough studies of the conversion of laser light into x rays with massive targets were performed by a number of workers,[9–21] covering a wide parameter range of laser intensity, pulse duration, wavelength, and target atomic number. The emission from thin gold layers, either free-standing or on a substrate, was investigated in Refs. 12, 19, and 22. From the measurements of Nishimura *et al.*[12,22] a characteristic burnthrough depth of ≈ 100 nm (at 10^{14} W/cm^2, wavelength 0.53 μm, and pulse duration 0.5–0.7 ns) has been inferred. Thin gold foils in this thickness range were recently used as x-ray converters.[2,3] The x rays emitted from the rear side provide an intense soft x-ray flux free of laser light if the converter foil is thick enough to absorb all the laser energy, but thin enough for an efficient x-ray flux to the rear. Such converter targets are an intense x-ray source for various experimental applications, which simultaneously avoid the drawbacks of direct laser radiation. Although the converter idea is not new, and in fact several experiments have already been carried out using this scheme as a basic component,[2,3] a detailed investigation of the converter itself including the x-ray emission towards the front and the rear and the transmission of laser light through the expanding foil has not yet been reported in the literature.

Figure 1 shows a sketch comparing the x-ray emission from a massive high-Z target with that from a thin converter foil. The conversion of laser light into x rays in massive targets has been analytically and numerically examined elsewhere,[23,24] yielding the following picture: The hot plasma in front of the cold target can be divided into two distinct regions, an optically thin conversion layer and an optically thick re-emission zone. The conversion layer is the outer low-density, high-temperature region, in which the laser light is absorbed and converted into x rays. The converted fraction is α_c, which is equally radiated in the two directions. The x rays propagating towards the solid target are absorbed in a region of high density and moderate temperature. This region is called the re-emission zone because some fraction $r < 1$ of the absorbed x rays is re-emitted. The total x-ray conversion fraction in massive targets η_x can then be expressed by $\eta_x = (1+r)\alpha_c/2$. The essential feature of a converter target is that it is so thin that it consists almost entirely of the conversion layer in order to obtain nearly symmetrical x-ray conversion fractions of $\alpha_c/2$ from each side of the target. With nanosecond pulses of submicrometer wavelength the total x-ray conversion from massive gold targets has been measured[19,21] to reach levels of up to $\approx 80\%$. Under these conditions the re-emission coefficient r approaches unity and one may then achieve up to 40% rear conversion fraction from a thin high-Z converter target. As will be shown, this qualitative picture appears to be confirmed by the experimental results presented below.

This paper reports an experimental investigation of x-ray emission from thin gold foils for 0.53-μm laser light

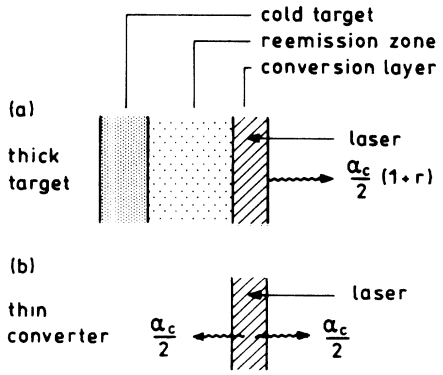

FIG. 1. A comparison of x-ray emission from high-Z targets in (a) the case of a thick target and (b) the case of a thin x-ray converter foil.

in a 3-ns pulse with simultaneous measurements of the laser light transmission through the target. The pulse length is significantly longer and the laser intensity lower than in the experiments with converter schemes reported up to now.[2,3,22] We can show that the thin foil converter functions equally successfully under these conditions, indicating that it may be a technique for general application. The experimental setup and the results are presented in Secs. II and III. The results are discussed in Sec. IV by comparing them with numerical hydrodynamic calculations. Special emphasis is given to the x-ray opacity of the hot converter foil.

II. EXPERIMENTAL ARRANGEMENT

The experiments were carried out with a Nd-glass laser frequency doubled to produce pulses of wavelength 0.53 μm, duration 3 ns, and energy 10 J. The laser beam was focused with $f/1.4$ optics onto the target, which was positioned behind the best focus to produce a diverging beam at the target surface. Two focal spot sizes were selected, a large one 630 μm in diameter yielding a laser intensity of $S_L = 10^{12}$ W/cm^2 and a smaller one 200 μm in diameter yielding a laser intensity of $S_L = 10^{13}$ W/cm^2. The local intensity on the target surface exhibits some structure, essentially consisting of concentric diffraction rings. The incident intensity pattern of the 630-μm spot is shown in Fig. 5(a) and is discussed in more detail in Sec. III B.

Two types of targets were used: free-standing gold foils and gold deposited on 1-μm polypropylene (CH_2, density 0.9 g/cm^3), referred to as "free-standing" and "supported" in the following. In addition, for comparison a number of target shots were carried out on thick (10-μm) gold foils, which may be considered as massive targets.

The experimental arrangement is shown schematically in Fig. 2. The x-ray emission was monitored with a set of two identical vacuum x-ray diodes, and two identical transmission x-ray grating spectrometers. These detectors were symmetrically placed at 30° from the target normal both in front of and behind the target. The x-ray diodes had copper cathodes and were filtered with 1.0-μm-thick polypropylene foils. They were primarily sensitive at wavelengths above the carbon K edge in the range 44 to 100 Å, and also at wavelengths < 30 Å significantly below the K edge. The combined diode-oscilloscope response time was ≈ 500 ps. For the spectral sensitivity of the cathode we used the data of Day *et al.*[25]

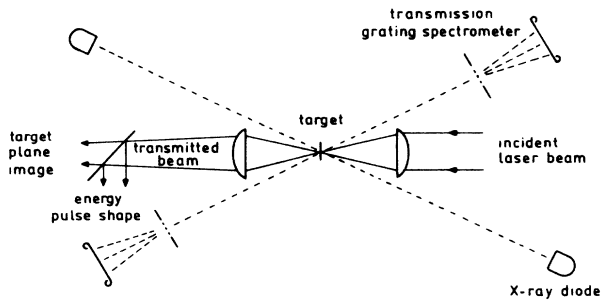

FIG. 2. Experimental arrangement for the x-ray converter foil investigation.

The spectrometers used identical gold transmission gratings with a grating period of 1 μm and absolutely calibrated Kodak 101-01 x-ray film as a detector. Details of this diagnostic can be found in Refs. 26 and 27. The spectral resolution was limited by the relatively large source size to 15 Å at intensity $S_L = 10^{12}$ W/cm^2 and 8 Å at $S_L = 10^{13}$ W/cm^2.

An $f/1$ lens placed behind the target plane was used to collect the directly transmitted laser light. In order to obtain spatial information from the transmitted beam, the target plane was imaged and recorded on burn paper with a spatial resolution better than 10 μm in the target plane. In addition, a set of energy diodes and a vacuum photodiode were used to monitor the transmitted energy and pulse shape from a signal split off from the main transmitted beam.

III. EXPERIMENTAL RESULTS

A. x-ray conversion

The total x-ray energy emitted towards the front and rear normalized to the incident laser energy is displayed in Fig. 3 as a function of the gold-layer thickness for free-standing and supported targets at the two laser intensities 10^{12} and 10^{13} W/cm^2. The general trend is towards a nearly symmetrical front and rear emission if the gold layers are very thin ($\lesssim 50$ nm). With thicker gold

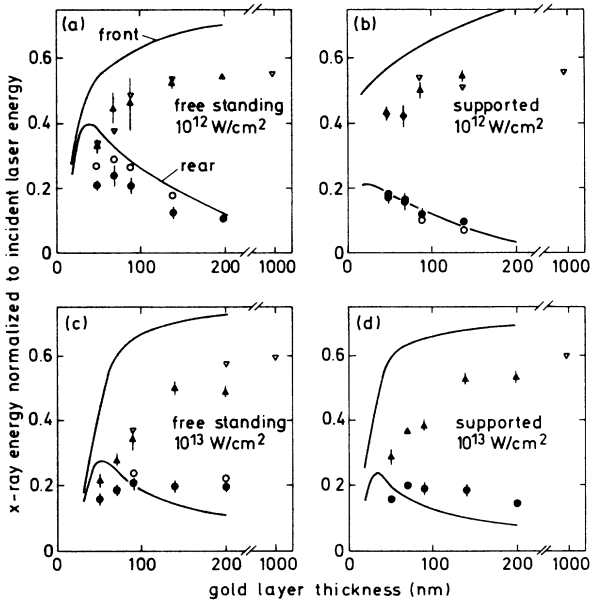

FIG. 3. Total x-ray emission from the front and rear sides of free-standing and supported converter targets at $S_L = 10^{12}$ and 10^{13} W/cm^2. Conversion measurements towards the front are denoted by triangles, and towards the rear by circles. The open and closed symbols were derived from film spectrometer measurements and x-ray diode signals, respectively. The solid curves represent simulation results.

layers, the front emission increases up to the massive target value, whereas the rear-side emission decreases. The maximum rear-side conversion efficiency approaches almost 30% for a free-standing gold foil; with supported targets, the rear-side conversion is somewhat smaller but still values of up to 20% were measured. A similar trend is seen in the numerical simulations (solid curves) discussed in Sec. IV.

The data points plotted in Fig. 3 were derived from spectra recorded on film (open symbols) and from diode signals (solid symbols). Absolute values of the emitted x-ray energy are obtained by analyzing the spectra recorded on film, taking into account the characteristic film gamma curve relating incident energy density to photographic density, and the wavelength dependence of the film sensitivity.[26,27] For the batch of Kodak 101-01 film actually used, recent calibration data were available.[28] The evaluated spectra were further corrected for contributions from the higher diffraction orders (amounting to a few percent). Integration of the spectra over the wavelength range 20–200 Å thereby yielded an absolute value for the emitted energy per unit solid angle as seen by the instrument.

Relative values of the emitted x-ray energy were formed from the diode signals by multiplying the signal peak level with the full width at half maximum (FWHM). These values were normalized to the absolute values obtained from the film spectra measured at the front side of massive targets.

Determination of the total x-ray energy requires that the angular distribution be known, but it was not measured in this experiment. We remember that for an optically thick blackbody radiator, the angular distribution follows the Lambertian cosine law, while for an optically thin volume radiator, it is independent of the angle. We assumed an isotropic angular distribution and therefore have calculated the data points in Fig. 3 by multiplying the x-ray energy measured by the detector at 30° to the target normal by the solid angle 2π of the half-space on each side of the target. For the converter targets we believe this to be a reasonable assumption because the very thin gold converter foil becomes a nearly optically thin source. With increasing target thickness the x-ray emitting region is no longer completely optically thin and deviations from an isotropic angular distribution are expected. Indeed, measurements of the angular distribution for massive gold targets show a dependence on angle.[11,21,27] Taking instead of an isotropic distribution the angular distribution measured by Kishimoto[27] for a massive gold target under irradiation conditions (3×10^{13} W/cm^2 at laser wavelength 0.53 μm and pulse duration 3 ns) similar to those of this experiment would result in 16% smaller values for the total x-ray energy. For example, the x-ray energy conversion efficiency at the front side of a massive target of 56% at $S_L=10^{12}$ W/cm^2 and 60% at $S_L=10^{13}$ W/cm^2 as plotted in Fig. 3 would then reduce to 47% and 50%. These massive target data are in good agreement with independent measurements recently performed in our laboratory[29] with a bolometer as detector, where 50%±5% energy conversion efficiency was measured at 10^{13} W/cm^2 and 60%±5% at 5×10^{13} W/cm^2 (with the same laser at wavelength 0.53 μm and pulse duration 3 ns).

B. Laser energy transmission

Measurements of the transmitted laser energy as a function of the gold-layer thickness for free-standing and supported targets are presented in Fig. 4(a) at $S_L=10^{12}$ W/cm^2 and in Fig. 4(b) at $S_L=10^{13}$ W/cm^2. In all cases the measured transmitted laser energy decreases with increasing gold-layer thickness. For free-standing targets at $S_L=10^{12}$ W/cm^2 and a gold-layer thickness in the region 70 to 90 nm, where maximum rear-side x-ray emission was observed, laser transmission is only a few percent, whereas larger values are observed at $S_L=10^{13}$ W/cm^2. In supported targets the polypropylene substrate significantly helps to reduce laser transmission.

In Fig. 5 we display the temporal pulse shape and spatial intensity distribution of the transmitted laser beam for various thicknesses of free-standing targets at 10^{12} W/cm^2. On the left of the figure are the incident and transmitted pulse shapes, and on the right the burn paper images of the intensity distribution of the transmitted beam in the target plane image. Both the incident and transmitted signals were recorded on the same oscilloscope trace with a fixed cable delay of 8 ns separating the two pulses. In Fig. 5(a) records are shown for the case of no target (full transmission) for comparison with Fig. 5(b), a 50-nm target, and Fig. 5(c), a 90-nm target. Filters were placed on the diodes to obtain a similar signal level for the incident and the transmitted beams. The transmitted laser light appears with a clear delay, which increases with target thickness.

The spatial intensity patterns of Fig. 5 contain considerable structure, which is already present in the incident beam shown in Fig. 5(a) in the case of no target. The

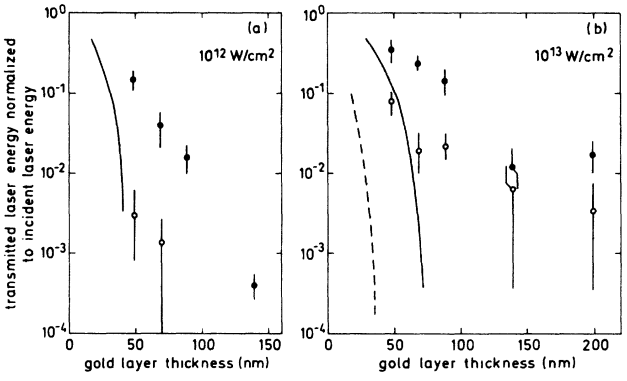

FIG. 4. Measurement and simulation results for the fraction of laser energy transmitted through converter targets. (a) Results at $S_L=10^{12}$ W/cm^2, with the solid symbols showing experimental measurements for free-standing targets, and the open symbols for supported targets. The solid curve shows the simulation results for free-standing targets; for supported targets the simulations showed no laser transmission for all gold thicknesses >20 nm. (b) The same as for (a) at $S_L=10^{13}$ W/cm^2; the dashed curve shows the simulation results for supported targets.

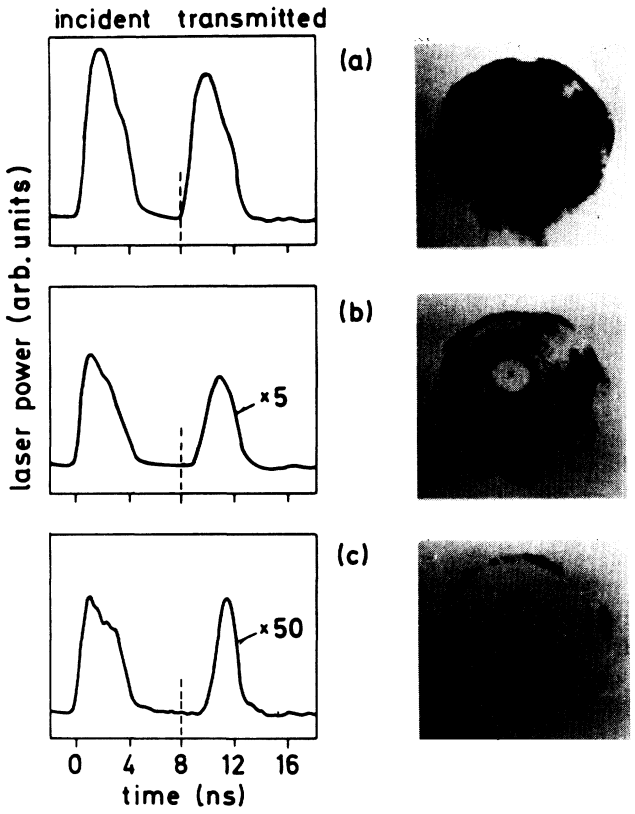

FIG. 5. Spatially and temporally resolved measurements of the transmitted laser beam at 10^{12} W/cm^2 for free-standing converter targets. On the left are oscilloscope traces of the incident and transmitted laser pulses. On the right are the burn paper images of the laser spot in the target plane. (a) Results for no target: the transmitted and incident pulses are the same; (b) results for a 50-nm gold target: the transmitted pulse is magnified by a factor of 5 by adjusting the entrance filter on the detector; (c) results for a 90-nm gold target: magnification of the transmitted laser pulse by a factor of 50.

concentric rings in the incident beam are caused by diffraction from apertures in the laser beam. The intensity on the diffraction rings in Fig. 5(a) is about a factor 2 larger than the average intensity. The region of low intensity in the center is caused by a hole in the focusing aspherical lens (necessary to avoid damage of the lens). The patterns Figs. 5(b) and 5(c) of the laser transmitted through thin converter foils show enhanced transmission primarily in regions in which the incident intensity is high. In Fig. 5(c) at thickness 90 nm the transmission apparently occurs only in the intense diffraction rings. The transmission patterns were reproducible from shot to shot. Aside from the differences in intensity, the ring pattern itself remained the same at all thicknesses. For supported targets at 10^{12} W/cm^2 the temporal and spatial measurements showed essentially the same features as the free-standing targets, but with generally much less laser transmission.

At $S_L = 10^{13}$ W/cm^2 the x-ray signals for both supported and free-standing targets showed a burnthrough delay similar to that at 10^{12} W/cm^2, although with signal onsets not as sharply defined. The spatial intensity distribution of the transmitted light did not display the structure of the incident beam as clearly as at 10^{12} W/cm^2. In addition, the patterns tended to vary with the target thickness: For thin targets it resembled the incident laser, while for thicker targets the overall pattern expanded in size and tended to clump into several large bundles. These patterns were also far less reproducible. This behavior indicates that refraction effects due to two-dimensional plasma expansion are important and also suggests that instabilities may be playing a role in beam breakup, as discussed in Sec. IV A.

We finally note that the amount of light reflected back through the focusing lens was less than 1%. For the long pulses and the relatively low intensity of this experiment, the total absorption measured with massive targets exceeds 90%.[12,30]

C. Spectrally and temporally resolved x-ray signals

1. *Free-standing targets*

Measurements of the spectra from both sides of the free-standing converter targets at $S_L = 10^{12}$ W/cm^2 are presented in Fig. 6 for three different target thicknesses. For the thinnest target [50 nm, Fig. 6(a)], the spectra from the front and rear are nearly the same except for the wavelength region below 50 Å, where the front spectrum is somewhat more intense. With increasing target thickness, the front spectra increase uniformly across the entire wavelength region. The rear spectra, however, exhibit a marked decrease in the total emission as well as a shift of the maximum in the 20–50 Å region to a broad peak around 60–110 Å.

Figure 7 shows time-resolved x-ray diode signals for the three target thicknesses of Fig. 6. Front and rear signals are recorded on the same oscilloscope trace with a fixed cable delay of 9.6 ns between them. The front-side signals have similar shapes with the amplitude increasing somewhat with target thickness. The signals emitted from the rear side of the targets show a shift of the peak to later times with increasing gold thickness, together with a noticeable increase in the rise time of the pulse. This trend of delayed maximum emission towards the rear continues for the 200-nm-thick gold foils (not shown). Within the limited time resolution (500 ps) of the diode, we did not see a delay in the onset of the emission towards the rear.

2. *Supported targets*

A comparison of the emission spectra of free-standing and supported targets shows little difference for the front-side spectra, but significant differences for the rear-side spectra. In Fig. 8 we compare the rear emission spectra from a free-standing (solid curve) and a supported (dashed curve) 70-nm gold layer. The filtering of the polypropylene (CH_2) substrate causes less emission to the rear, especially at shorter wavelengths below the carbon K edge (at 44 Å for cold carbon). As an additional comparison, we display the measured rear emission from a free-standing 70-nm gold target filtered by a cold 1-μm-

thick polypropylene foil placed at a large distance from the target in front of the spectrometer grating (dashed-dotted curve). The observed filtering is as expected from the absorption coefficient[31] of cold polypropylene (essentially carbon). The supported target spectrum (dashed curve) is more intense at each wavelength than the filtered free-standing target spectrum (dashed-dotted curve). We discuss these results in Sec. IV B 2 taking into account the opacity of the substrate material, which is heated by the x rays.

Time-resolved x-ray diode signals of the rear emission for this example are displayed in Fig. 9. Here, the solid curve shows the emission from the 70-nm free-standing target, and the dashed curve that from the supported target of the same gold thickness. The front pulse shapes are essentially identical (the slight differences noticeable here being caused by shot-to-shot variations of the incident laser pulse). However, the rear signals from the free-standing and the supported targets show characteristic differences. At the beginning of the pulse the signal of the supported target is somewhat less than 50% of the free-standing target signal, whereas at later times after the peak of the pulse the emission from the supported target approaches that of the free-standing target, i.e., the substrate has become gradually more transparent.

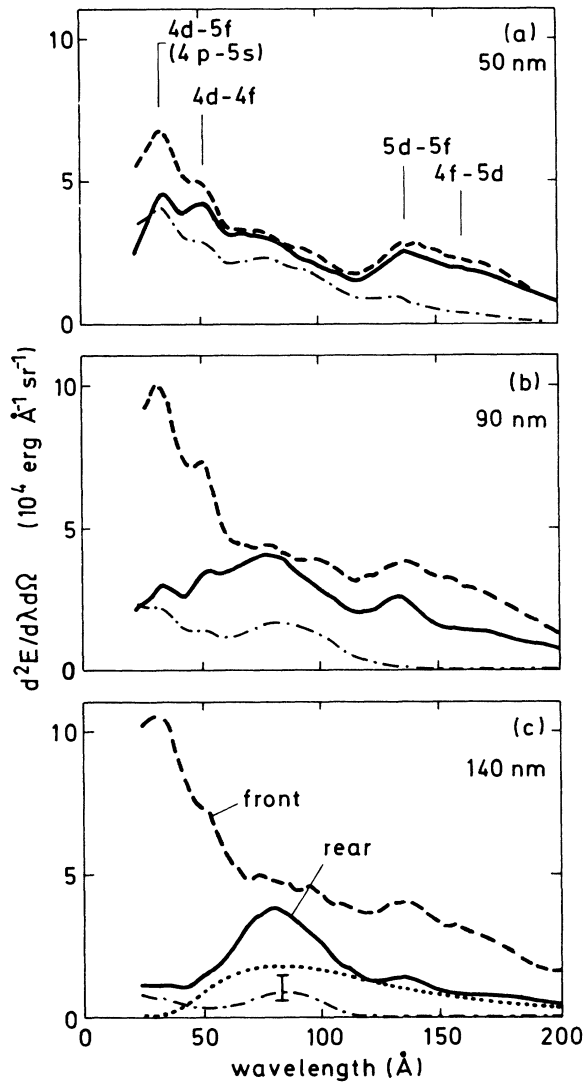

FIG. 6. Transmission grating spectra of the front and rear x-ray emission at 10^{12} W/cm^2 for free-standing gold targets. The dashed curves are the front spectra and the solid curves are the rear spectra. Target thicknesses are (a) 50 nm, (b) 90 nm, and (c) 140 nm. The dashed-dotted curves are calculated from the measured front spectra and show these as they would be seen transmitted through a cold gold filter of thickness in (a) 20 nm, (b) 60 nm, and (c) 110 nm. The dotted curve in (c) is a calculated Planck spectrum for temperature 30 eV.

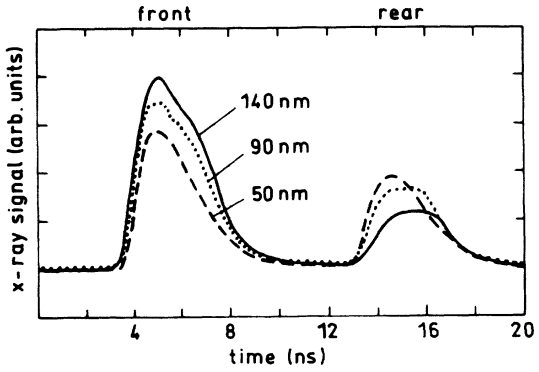

FIG. 7. Oscilloscope traces of the front and rear x-ray diode signals at $S_L = 10^{12}$ W/cm^2 for free-standing gold targets with the same three thicknesses as in Fig. 6 are displayed: dashed, 50 nm; dotted, 90 nm; solid, 140 nm gold thickness.

IV. DISCUSSION

A. Comparison with numerical simulations

Simulations of thin converter targets were performed with MULTI,[32] a planar, Lagrangian, one-dimensional, fully implicit code which solves the hydrodynamic equa-

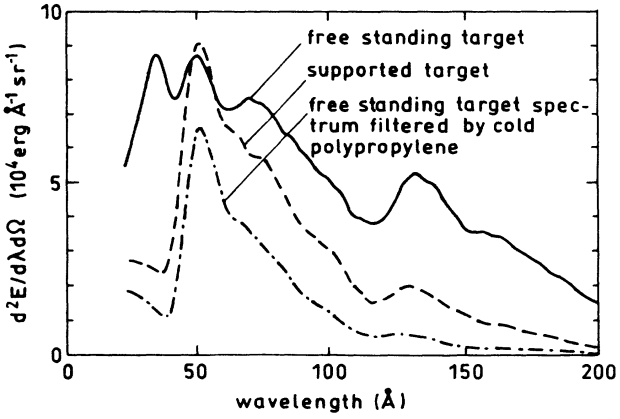

FIG. 8. Measurement of x-ray spectra on the rear side of a free-standing and a supported target: gold thickness 70 nm, $S_L = 10^{12}$ W/cm^2. For comparison the spectrum from a free-standing target filtered by 1-μm cold polypropylene is also shown.

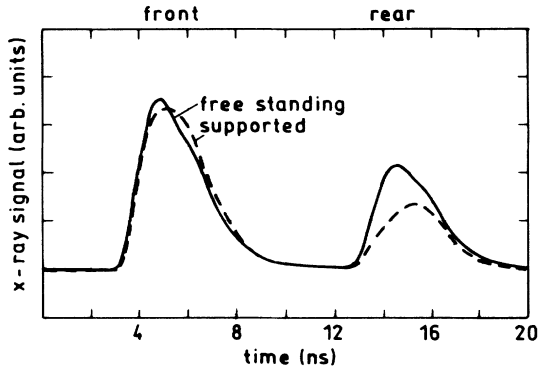

FIG. 9. Comparison of oscilloscope traces of x-ray diode signals on the rear side of 70-nm gold targets at $S_L = 10^{12}$ W/cm^2: solid, free-standing target; dashed, supported target.

tions coupled with multigroup radiation transport. The laser energy is absorbed by inverse bremsstrahlung. The remaining laser flux reaching the critical density layer was deposited there, causing 100% absorption as long as the plasma is above critical density. Flux-limited electron heat conduction was used with the flux limiter set to 0.08. X-ray emission and absorption coefficients as well as the plasma ionization state were calculated in a steady-state non-local-thermodynamic-equilibrium approximation.[33] A detailed discussion of results for massive gold targets obtained with the MULTI code is given in Ref. 24.

Simulation results of the rear and the front conversion efficiencies as functions of the gold-layer thickness are shown by the solid curves in Fig. 3. The calculated laser light transmission is given by the curves in Fig. 4.

To illustrate the simulations, we have displayed in Fig. 10 spatial temperature and density profiles for different thicknesses of free-standing gold foils. The profiles represent snapshots at a fixed time which corresponds to the maximum of the laser pulse ($S_L = 10^{12}$ W/cm^2).

Very thin foils [20 nm in Fig. 10(a)] rapidly expand to low densities and become underdense early in the beginning of the laser pulse. Some fraction of the incident laser energy is absorbed by inverse bremsstrahlung in the underdense plasma, the rest of about 50% [see Fig. 4(a)] being transmitted. This situation results in an almost isothermal temperature and a Gaussian density profile. It resembles very closely that of exploding-foil experiments, which have been extensively investigated in connection with x-ray laser schemes.[34] Front and rear x-ray signals emitted by the nearly symmetrically expanding, optically thin plasma are almost identical. In terms of the simple picture described by the sketch of Fig. 1, the plasma in this case consists of just a conversion layer.

In the other extreme of relatively thick targets, the division of the target into a hot conversion layer (CL) and a cooler absorption and re-emission zone (RZ) is clearly apparent in the simulations [see Fig. 10(c)]. Here the 300-nm gold layer is thick enough to absorb the radiation generated in the conversion zone. The energy is transported in the re-emission zone by an ablative radiative heat wave[35] propagating at the front of the re-emission

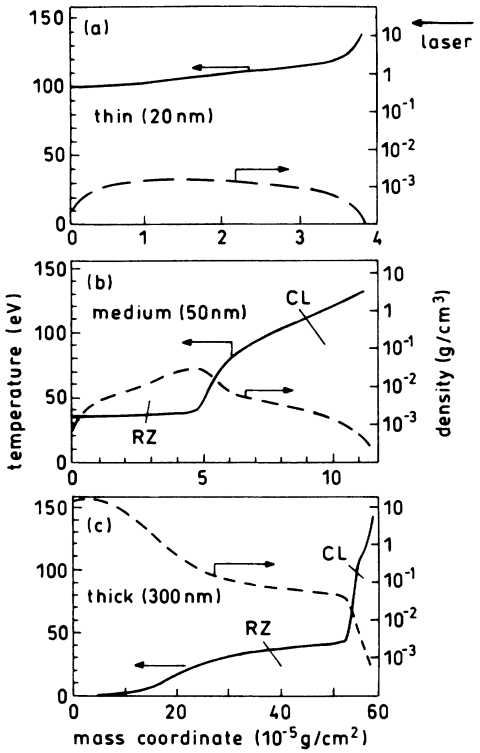

FIG. 10. Calculated temperature and density profile in a 20, 50, 300-nm-thick free-standing gold foil, $S_L = 10^{12}$ W/cm^2.

zone. In Fig. 10(c) the radiative heat wave has not yet reached the rear side of the target, which is therefore still close to the solid-state density (at a temperature of about 0.3 eV owing to shock heating). The front emission is enhanced by the re-emission and approaches the level expected for a massive target, while the rear emission is small.

In the medium range between these extremes there lies an optimum target thickness for obtaining maximum emission towards the rear. According to Fig. 3, this optimum thickness is at 40 to 50 nm. The density and temperature profiles in Fig. 10(b) (50-nm foil) indicate the existence of a narrow re-emission zone. The density in this zone is high enough to avoid laser light transmission which only becomes significant at the end of the pulse, when the foil is more decompressed. Owing to the larger amount of deposited laser energy, the rear emission shows a maximum which, according to the simulation, is 40% of the laser energy for $S_L = 10^{12}$ W/cm^2 and a free-standing gold foil.

In the simulations for supported targets we modeled the substrate as a pure carbon layer of initial thickness 1 μm and density 1 g/cm^3. The results presented in Fig. 3 show a smaller emission towards the rear compared with free-standing targets,which stems mainly from absorption of x rays in the substrate, as discussed in more detail in Sec. IV B 2. The transmission of laser light in supported targets is much less than in free-standing targets (see Fig. 4). This is caused by absorption of laser light in the ionized substrate material. Furthermore, the presence of the substrate prevents free expansion of the gold layers close to the carbon-gold interface and increases somewhat the

gold density, which also helps to reduce laser light transmission.

The comparsion between simulations and measurements in Figs. 3 and 4 shows that several experimental trends are qualitatively described by the theoretical modeling: For the thinnest free-standing gold layers (50 nm) we measure approximately a symmetrical back and front emission, which is also seen in the spectra and the pulse shapes displayed in Figs. 6(a) and 7; with increasing gold-layer thickness, the front emission increases up to the massive target value, whereas the rear emission decreases (at least at 10^{12} W/cm^2). In supported targets the rear conversion is slightly reduced; the laser transmission decreases and occurs delayed with increasing gold-layer thickness and is considerably smaller in supported than in free-standing targets.

In detail, however, one observes in Figs. 3 and 4 quantitative discrepancies, which are attributed to several approximations made in the simulations. One reason is certainly the simplified atomic physics model[33] used. In the context of the radiative transport in the target, this will be discussed in more detail in Sec. IV B.

Another approximation made is the one-dimensional plane geometry. Deviations from this ideal case may be caused by the nonuniform intensity distribution of the laser beam. This creates local burnthrough as observed experimentally in Fig. 5. Also thermal self-focusing may be important and may be the reason for the nonreproducible intensity distribution of the transmitted laser light observed at $S_L = 10^{13}$ W/cm^2. These effects could be responsible for the measured laser light transmission being considerably larger than in the simulation (see Fig. 4). They also may cause the shift of the maximum rear conversion to larger gold-layer thicknesses in the experiment compared with the simulation. In view of the rather poor laser focal spot quality in the experiment, we believe that the results can be significantly improved with a smoother intensity distribution in the laser focal spot in order to obtain higher rear conversion at less laser transmission.

Lateral expansion at the front and the rear side is also not considered in the one-dimensional calculations. This could be of importance especially at $S_L = 10^{13}$ W/cm^2 with the smaller laser spot of 200 μm (compared to 600 μm at $S_L = 10^{12}$ W/cm^2). From the plasma parameters found in the simulations [$Z \approx 20$ (40), $T \approx 100$ (500) eV at $S_L = 10^{12}$ (10^{13}) W/cm^2], we calculate a sound speed of $c_s = (ZT/M)^{1/2} \approx 3 \times 10^6$ cm/s for 10^{12} W/cm^2 and $\approx 10^7$ cm/s for 10^{13} W/cm^2. For the $\tau = 3$ ns laser pulse duration the expansion scale length is $c_s \tau \approx 100$ μm at $S_L = 10^{12}$ W/cm^2, which is roughly a sixth of the spot diameter. At $S_L = 10^{13}$ W/cm^2 the expansion scale length reaches $c_s \tau \approx 300$ μm, significantly larger than the 200-μm laser spot diameter. In this case the foil expands spherically rather than in one dimension, which allows the laser to penetrate deeper than expected from one-dimensional simulations. This is consistent with the observations of large laser transmission through thicker targets, especially at 10^{13} W/cm^2. The large fraction of transmitted laser energy also contributes to direct laser heating of parts of the rear surface, as confirmed by the fact that the measured rear conversion at 10^{13} W/cm^2 lies above the curves calculated in the one-dimensional simulations. The detailed observations of the intensity distribution of the transmitted laser beam also indicated the presence of significant refraction, as would be expected in a spherically shaped plasma cloud.

B. Radiation emission and transport

1. Free-standing targets

Simulated front and rear time-integrated spectra for three free-standing target thicknesses (50, 90, 140 nm) at $S_L = 10^{12}$ W/cm^2 are displayed in Fig. 11. In addition, the insets show the frequency-integrated x-ray pulses emitted towards the front and rear sides. The rear emission sets in after some delay when the rear side of the target is heated up by the radiative heat wave. The delay increases with the target thickness and the peak emission of the rear spectra shifts somewhat to longer wavelengths, because the rear side in thicker targets is considerably

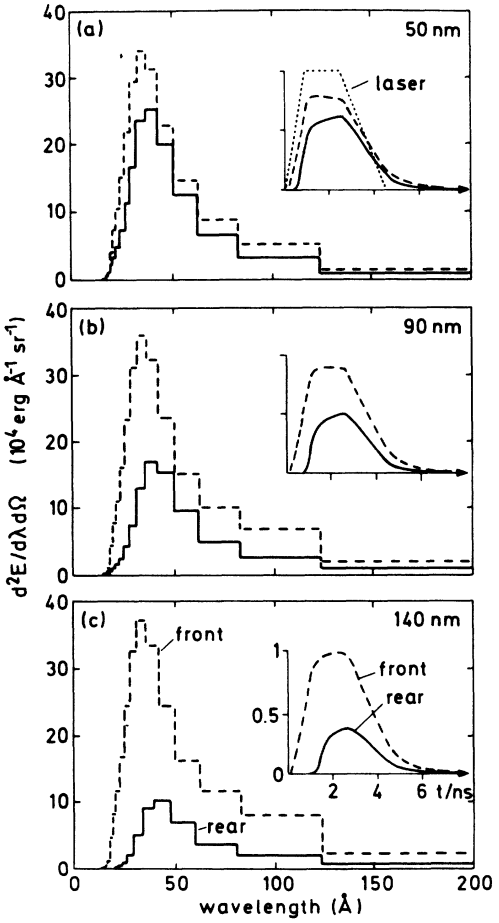

FIG. 11. Simulated x-ray spectra of the front and rear x-ray emission at 10^{12} W/cm^2 for free-standing gold targets. The dashed curves are the front spectra and the solid curves are the rear spectra. Target thicknesses are (a) 50 nm, (b) 90 nm, and (c) 140 nm. The insets show the calculated frequency-integrated front and rear x-ray pulses in arbitrary units [in (a) the laser pulse is also plotted].

colder than the front side (see Fig. 10).

Figure 11 may be directly compared with the experimental spectra and x-ray pulses shown in Figs. 6 and 7. As a common trend of the calculated and the measured spectra, the shape of the front spectra does not change much with gold thickness, whereas the rear spectra show a shift to longer wavelengths with increasing target thickness. In detail, however, discrepancies between simulation and experiment are evident. The experimental spectra show much more structure than the calculated ones. In the measured rear x-ray pulses we observe a delay only for the pulse maximum, whereas the onset of the signal occurs in contrast to the simulations without a delay even for the thickest targets studied. This could be caused by local burnthrough in the hot spots of the laser beam as observed for thinner targets. However, at the lower intensity $S_L = 10^{12}$ W/cm^2 considered here, burnthrough was negligible for thicker targets ($\gtrsim 140$ nm). The instantaneous onset of the rear signal may therefore indicate that directly transmitted x rays from the hot laser-heated conversion layer at the front side are important, as discussed below.

One major reason for the disagreement between simulation and experiment is the simplifying assumptions made for the theoretical opacities.[33] They are calculated within a hydrogenlike approximation, which describes the energy levels of the gold ions by the principal quantum number only. The peak in the simulated spectra at about 35 Å is essentially caused by 4–5 bound-bound transitions. However, as pointed out by several workers,[36,37] l splitting is important for the spectra of complex ions. On the basis of theoretical calculations[38–41] of the subshell energy levels for differently charged ions, we identified the peaks in the measured front spectra as bound-bound transitions between subshells and have noted this in Fig. 6(a). An average charge state of the gold ions $Z \approx 20$ was used, which is expected for $S_L = 10^{12}$ W/cm^2, according to the simulations.

We now turn to the measured rear spectra. For the thinnest target [50 nm, Fig. 6(a)] the rear spectrum does not deviate much from the front spectrum, because this target is nearly optically thin. This situation essentially corresponds to the case of optimum converter foil thickness with maximum emission to the rear side. In thicker targets the radiative transport becomes important. The rear spectra of these targets with a more inhomogeneous temperature and density distribution may contain contributions from the hot plasma at the front side and the colder plasma at the rear side. Simulations indicate a temperature of 30 eV at the rear side of the target after the radiative heat wave has propagated through the foil. If it is assumed that this region is optically thick, a Planck spectrum would be radiated as shown by the dotted line in Fig. 6(c) for $kT = 30$ eV. The 30-eV Planck spectrum is a considerable fraction of the measured rear spectrum and is at wavelengths $\gtrsim 100$ Å approximately in agreement with the measured spectrum. Thus one may conclude that the radiation emitted toward the rear to a large extent is caused by self-emission from the rear target side, which is heated by the radiative heat wave.

As already inferred from the measured rear x-ray pulse, directly transmitted radiation from the hot front side may also contribute to the rear emission. Direct transmission is possible in spectral regions, in which the target is not optically thick enough. This may be the case in the spectral region below ≈ 100 Å, where the measured spectrum is above the Planck spectrum. At ≈ 80 Å we observe for thicker targets the formation of a characteristic peak [see Fig. 6(c)]. It appears in a spectral region where the photoionization cross section of cold solid gold[31,42] exhibits a broad minimum centered at ≈ 80 Å, which is mainly a consequence of the behavior of the $4f$ and $5d$ subshell photoionization cross sections.[40] Thus one would expect a peak at ≈ 80 Å in the rear spectra when one assumes that the radiation from the hot laser-heated conversion layer at the front side is filtered by the remainder of the target acting as a cold gold filter. The dashed-dotted spectra in Fig. 6 are calculated in this way from the front spectra with the cold gold opacity as given by Henke *et al.*[31] As the thickness of the cold gold filter we took the target thickness minus an estimated thickness of 30 nm for the laser-heated conversion layer. The error bar in Fig. 6(c) indicates the existing uncertainty in the cold gold opacity data,[42] which especially around the minimum at 80 Å is rather large (about a factor 2).

The dashed-dotted spectra show as the experimental spectra the formation of a peak at ≈ 80 Å, but at a considerably lower level [see Fig. 6(c)]. This may be caused by heating and ionization of the rear target material by the absorbed x rays, which leads to a reduction of the absorption by photoionization because the ionized gold has fewer bound electrons than cold gold and higher ionization thresholds for the different subshells. As a result, the heated target material becomes more transparent than cold gold. Duston *et al.*[43] observed transmission enhanced by this effect in a computational study of a laser-irradiated aluminum target and called it "ionization burnthrough."

From the above discussion it becomes clear that the radiation emitted from laser-irradiated thin gold foils is of interest to check opacity models implemented in hydrodynamic simulations. We find that a more realistic description than is given by the present simulations would require more precise opacity calculations including, for example, l-splitting effects.

2. *Supported targets*

Typically, the supported targets yielded less rear emission than free-standing targets, which we attribute to absorption of the radiation emitted by the gold layer in the substrate. Self-emission from the relativity cold low-Z plasma of the substrate is of minor importance.

We now discuss this aspect in somewhat more detail because it gives information on the absorption of radiation in the hot dense carbon plasma of the substrate. The opacity of the substrate material was calculated from the measured rear spectra (Fig. 8) of the free-standing and the supported target resulting in the experimental points plotted in Fig. 12. We neglected changes of the substrate mass per area (g/cm^2) by lateral expansion, which is reasonable for the large laser spot of the laser intensity

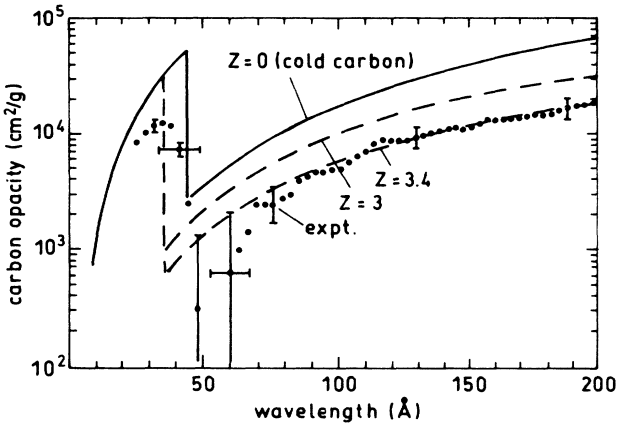

FIG. 12. Carbon opacity vs wavelength: solid dots, experimental opacity of the heated polypropylene (CH_2) substrate as determined from the measured spectra in Fig. 8; solid curve, cold carbon opacity (Ref. 31); dashed curve, theoretical carbon opacity (Ref. 44) for ionization states $Z=3$ and $Z=3.4$.

10^{12} W/cm^2 considered here (see Sec. IV A). It was also assumed that the rear spectrum emitted by the free-standing target (measured in a different shot) is identical with that of the radiation entering the substrate in the case of the supported target. Certainly this assumption is not quite correct for wavelengths $\lambda \approx 50$ Å, where the intensity with the supported target is even a little bit higher than with the free-standing target (see Fig. 8). This could be caused by small shot-to-shot variations or small changes of the gold emission due to the presence of the substrate. Greater uncertainty therefore exists in the measured opacity at $\lambda \approx 50$ Å.

The measured opacity is lower (by a factor of about 3 at wavelengths above the K edge of carbon) than the cold carbon opacity. This is attributed to ionization of the substrate. According to the experiment and the simulations, the amount of x-ray energy deposited in the substrate is about 10% of the laser energy, which heats the substrate to temperatures of 10 to 20 eV. At the same time the substrate decompresses, reaching densities of 10^{-2} to 10^{-3} g/cm^3 at the end of the laser pulse. The typical ionization state of the carbon ions is between 3 and 4.

The photoionization cross section taken for the hydrodynamic simulation[33] was approximated by Kramer's formula, in which the wavelength scaling of the opacity is proportional to λ^3. However, this scaling describes the experimental result poorly. A more accurate calculation of the absorption by photoionization was performed by Reilman and Manson.[44] These theoretical results were recently confirmed experimentally for beryllium ions[45] and for carbon ions.[46] In Fig. 12 we plotted the opacity according to Reilman and Manson for C^{3+} ions [$Z=3$; for neutral carbon ($Z=0$) their result is in agreement with the data of Henke *et al.*[31] for cold solid carbon]. At wavelengths above the carbon K edge the absorption is caused by photoionization of L-shell electrons. In this region the opacity of C^{3+} is smaller than for C^0 mainly because of the different numbers of electrons in the L shell. The K edge of C^{3+} is shifted to smaller wavelengths because of less screening by L-shell electrons. At wavelengths below the K edge the absorption is not influenced by the ionization of the L shell and the cross sections for C^0 and C^{3+} coincide.

At wavelengths above the K edge, the experimental opacity is lower than the theoretical[44] opacity for C^{3+}. This indicates that the degree of ionization is larger than three and that C^{4+} ions are present in the plasma in addition to C^{3+} ions (note that the photoionization cross section for C^{4+} is zero for wavelengths above the K edge because the L shell is empty). Assuming an average charge $Z=3.4$ in reasonable agreement with the charge state expected from the simulations, we find a good coincidence between theoretical and experimental opacities in a wide range of wavelengths $80 \leq \lambda \leq 200$ Å, which may be considered as a confirmation of the theoretical photoionization cross sections of Reilman and Manson.

In the region around the carbon K edge, the experimental wavelength resolution is not high enough to make definite statements. The measured position of the edge does not seem to be as strongly shifted to shorter wavelengths as the theoretical K edge for $Z=3$ or 4. This may be caused by continuum lowering (the calculations of Reilman and Manson[44] refer to an isolated carbon atom) and/or by K-shell absorption lines which are not resolved at the present spectral resolution (the absorption line with the largest wavelength is the $1s^2$-$1s2p$ transition, which is at 40.3 Å in C^{4+}).

V. SUMMARY

We have presented a detailed study of the radiation emission towards the front and the rear sides of thin gold foils to be used as efficient converters of laser light into x rays. We find an optimum gold thickness for maximum conversion towards the rear with low laser transmission. For the laser parameters of our experiments (intensity 10^{12} to 10^{13} W/cm^2 at pulse duration 3 ns and wavelength 0.53 μm) we measure with free-standing gold foils ≈ 70 nm thick a maximum conversion efficiency of up to 30% with only a few percent laser light transmission, mainly in hot spots of the laser beam. The laser light transmission could certainly be reduced by a more uniform laser illumination.

Considerably less laser transmission was found with thin gold layers supported on a 1-μm-thick polypropylene substrate, whereas the maximum x-ray conversion decreased only slightly. Supported targets are also advantageous for a slower material flow to the rear. This is important in experiments (such as x-ray laser pumping or opacity studies) in which the rear emission from the converter foil is used to heat a second target. One could also change the material of the conversion layer and of the substrate (not done in this work) in order to optimize the shape of the emitted rear spectra for special applications.

As an interesting aspect, we discussed the results with respect to the opacity of the hot dense converter foil material. Numerical simulations with the MULTI hydrocode described well the characteristic trends of the overall conversion efficiency. However, the detailed spectral and

temporal behavior of the emission showed differences between the simulations and the experiment, which were interpreted as a consequence of insufficiently detailed gold opacities used in the simulations. In particular, consideration of the strong l splitting of the N and O shells seems to be important.

In the case of the supported targets we found increased transmission of radiation through the heated polypropylene substrate compared with the cold substrate, which was explained as a decrease of the photoionization cross section due to the ionization of the polypropylene. We note that measurements of the photoionization cross section in hot dense matter (with the exception of Refs. 45 and 46 for plasmas at lower densities) have not been performed previously.

Future experiments with improved experimental setups[3] and better spectral resolution would certainly be of interest for the study of opacities in hot dense matter. For high-Z targets such as gold a separate measurement of the contributions caused by self-emission and by directly transmitted light would be important.

ACKNOWLEDGMENTS

The authors would like to thank R. Fedosejevs, R. Sigel, and G. D. Tsakiris for helpful discussions and S. Witkowski for his continuous support and interest in this work. They appreciate the assistance of A. Böswald in operating the Nd laser and the assistance of W. Fölsner in producing well-characterized thin foil targets. This work was supported in part by the Commission of the European Communities in the framework of the EURATOM—Max-Planck-Institut für Plasmaphysik Association.

---

*Permanent address: Department of Physics, University of British Columbia, Vancouver, Canada V6T 2A6.

[1]E. Storm, J. Fusion Energy **7**, 131 (1988).

[2]T. Mochizuki, K. Mima, N. Ikeda, R. Kodama, H. Shiraga, K. A. Tanaka, and C. Yamanaka, Phys. Rev. A **36**, 3279 (1987).

[3]S. J. Davidson, J. M. Foster, C. C. Smith, K. A. Warburton, and S. J. Rose, Appl. Phys. Lett. **52**, 847 (1988).

[4]C. Chenais-Popovics, C. Fieret, J. P. Geindre, and J. C. Gauthier, in *X Rays from Laser Plasmas,* edited by Martin C. Richardson (SPIE, Bellingham, WA, 1988), Vol. 831, p. 30.

[5]T. Endo, H. Shiraga, K. Shihoyama, and Y. Kato, Phys. Rev. Lett. **60**, 1022 (1988).

[6]D. G. Goodwin and E. E. Fill, J. Appl. Phys. **64**, 1005 (1988).

[7]F. O'Neill, G. M. Davis, M. C. Gower, I. C. E. Turcu, M. Lawless, and M. Williams, in *X-Rays from Laser Plasmas,* edited by Martin C. Richardson (SPIE, Bellingham, WA, 1988), Vol. 831, p. 230.

[8]M. Kühne and H.-Ch. Pelzold, Appl. Opt. **27**, 3926 (1988).

[9]M. F. Rosen, D. W. Phillion, V. C. Rupert, W. C. Mead, W. L. Kruer, J. J. Thomson, H. N. Kornblum, V. W. Slivinsky, G. J. Caporaso, M. J. Boyle, and K. G. Tirsell, Phys. Fluids **22**, 2020 (1979).

[10]P. D. Rockett, W. Priedhorsky, and D. Giovanielli, Phys. Fluids **25**, 1286 (1982).

[11]W. C. Mead, E. M. Campbell, K. G. Estabrock, R. E. Turner, W. L. Kruer, P. H. Y. Lee, B. Prutt, V. C. Rupert, K. G. Tirsell, G. L. Stradling, F. Ze, C. E. Max, M. D. Rosen, and B. F. Lasinski, Phys. Fluids **26**, 2316 (1983).

[12]H. Nishimura, F. Matsuoka, M. Yagi, K. Yamada, S. Nakai, G. H. McCall, and C. Yamanaka, Phys. Fluids **26**, 1688 (1983).

[13]T. Mochizuki, T. Yabe, K. Okada, M. Hamada, N. Ikeda, S. Kiyokama, and C. Yamanaka, Phys. Rev. A **33**, 525 (1986).

[14]R. Kodama, K. Okada, N. Ikeda, M. Mineo, K. A. Tanaka, T. Mochizuki, and C. Yamanaka, J. Appl. Phys. **59**, 3050 (1986).

[15]P. Alaterre, H. Pèpin, R. Fabbro, and B. Faral, Phys. Rev. A **34**, 4184 (1986).

[16]K. Eidmann and T. Kishimoto, Appl. Phys. Lett. **49**, 377 (1986).

[17]H. N. Kornblum, R. L. Kauffman, and J. A. Smith, Rev. Sci. Instrum. **57**, 2179 (1986).

[18]H. C. Gerritsen, H. van Brug, F. Bijkerk, and M. J. van der Wiel, J. Appl. Phys. **59**, 2337 (1986).

[19]P. D. Goldstone, S. R. Goldman, W. C. Mead, J. A. Cobble, G. Stradling, R. H. Day, A. Hauer, M. C. Richardson, R. S. Marjoribanks, P. A. Jaanimagi, R. L. Keck, F. J. Marshall, W. Seka, O. Barnouin, B. Yaakobi, and S. A. Letzring, Phys. Rev. Lett. **59**, 56 (1987).

[20]R. Sigel, K. Eidmann, J. Meyer-ter-Vehn, G. D. Tsakiris, and S. Witkowski, in *X Rays from Laser Plasmas,* edited by Martin C. Richardson (SPIE, Bellingham, WA, 1988), Vol. 831, p. 73.

[21]W. C. Mead, E. K. Stover, R. L. Kauffmann, H. N. Kornblum, and B. F. Lasinski, Phys. Rev. A **38**, 5275 (1988).

[22]H. Nishimura, T. Yabe, T. Endo, K. Kondo, H. Shiraga, Y. Kato, and S. Nakai, in *Short-wavelength Lasers and their Applications,* Vol. 30 of *Springer Proceedings in Physics,* edited by C. Yamanaka (Springer-Verlag, Berlin, 1987), p. 261.

[23]R. Sigel, K. Eidmann, F. Lavarenne, and R. Schmalz, Phys. Fluids B **2**, 199 (1990).

[24]K. Eidmann, R. F. Schmalz, and R. Sigel, Phys. Fluids B **2**, 208 (1990).

[25]R. H. Day, P. Lee, E. B. Saloman, and D. J. Nagel, Los Alamos Report No. LA-7941-MS, 1981 (unpublished).

[26]K. Eidmann, T. Kishimoto, P. Herrmann, J. Mizui, R. Pakula, R. Sigel, and S. Witkowski, Laser and Particle Beams **4**, 521 (1986).

[27]T. Kishimoto, dissertation, Ludwig-Maximilians-Universität München, 1986 (Report No. MPQ 108, 1985, Max-Planck-Institut für Quantenoptik, Garching bei München, Federal Republic of Germany).

[28]W. Schwanda and K. Eidmann (unpublished).

[29]K. Eidmann and W. Schwanda (unpublished).

[30]C. Garbana-Labaune, E. Fabre, C. Max, F. Amiranoff,R. Fabbro, J. Virmont, and W. C. Mead, Phys. Fluids **28**, 2580 (1985).

[31]B. L. Henke, P. Lee, T. J. Tanaka, R. L. Shimabukuro, and B. K. Fujikawa, At. Data Nucl. Data Tables **27**, 1 (1982).

[32]R. Ramis, R. Schmalz, and J. Meyer-ter-Vehn, Comput. Phys. Commun. **49**, 475 (1988).

[33]K. Eidmann, in *Course and Workshop of the International School of Plasma Physics Piero Caldirola "Inertial Confinement Fusion," Varenna, 1988,* edited by A. Caruso and E. Sindoni (Editrice Compositori, Bologna, Italy, 1989),

p. 65.
[34]R. A. London and M. D. Rosen, Phys. Fluids **29**, 3813 (1986).
[35]R. Pakula and R. Sigel, Phys. Fluids **28**, 232 (1985); **29**, 1340E (1986).
[36]T. Yabe and C. Yamanaka, Comments Plasma Phys. Controlled Fusion **9**, 169 (1985).
[37]D. G. Stearns, O. L. Landen, E. M. Campbell, and J. H. Scofield, Phys. Rev. A **37**, 1684 (1988).
[38]J. A. Bearden and A. F. Burr, Rev. Mod. Phys. **39**, 125 (1967).
[39]T. A. Carlson, C. W. Nestor, Jr., N. Wasserman, and J. D. McDowell, At. Data Nucl. Data Tables **2**, 63 (1970).
[40]J. J. Yeh and I. Lindau, At. Data Nucl. Data Tables **32**, 1 (1985).
[41]T. Yabe (private communication).
[42]E. B. Saloman, J. H. Hubbel, and J. H. Scofield, At. Data Nucl. Data Tables **38**, 1 (1988).
[43]D. Duston, R. W. Clark, J. Davis, and J. P. Apruzese, Phys. Rev. A **27**, 1441 (1983).
[44]R. F. Reilman and S. T. Manson, Astrophys. J. Suppl. Ser. **40**, 815 (1979).
[45]E. Jannitti, P. Nicolosi, G. Tondello, Zheng Yongzhen, and M. Mazzoni, Opt. Commun. **63**, 37 (1987).
[46]G. Tondello (private communication).

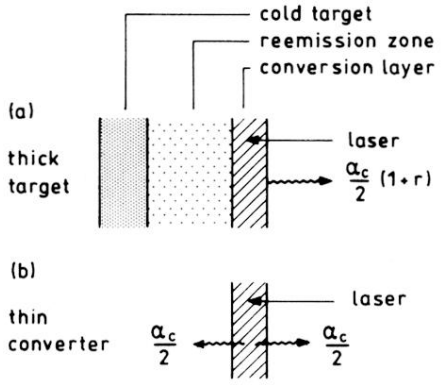

FIG. 1. A comparison of x-ray emission from high-Z targets in (a) the case of a thick target and (b) the case of a thin x-ray converter foil.

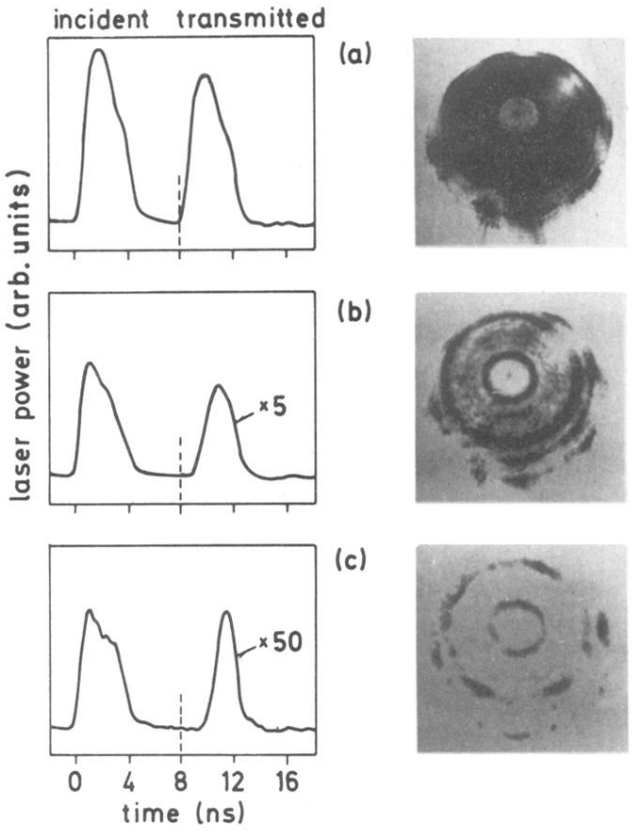

FIG. 5. Spatially and temporally resolved measurements of the transmitted laser beam at 10^{12} W/cm^2 for free-standing converter targets. On the left are oscilloscope traces of the incident and transmitted laser pulses. On the right are the burn paper images of the laser spot in the target plane. (a) Results for no target: the transmitted and incident pulses are the same; (b) results for a 50-nm gold target: the transmitted pulse is magnified by a factor of 5 by adjusting the entrance filter on the detector; (c) results for a 90-nm gold target: magnification of the transmitted laser pulse by a factor of 50.